New Journal of Physics
The open access journal at the forefront of physics

Deutsche Physikalische Gesellschaft DPG
IOP Institute of Physics

Published in partnership with: Deutsche Physikalische Gesellschaft and the Institute of Physics

OPEN ACCESS

RECEIVED
15 September 2020

REVISED
16 December 2020

ACCEPTED FOR PUBLICATION
31 December 2020

PUBLISHED
20 January 2021

PAPER

Enhancement of quantum synchronization via continuous measurement and feedback control

Yuzuru Kato* and **Hiroya Nakao**

Department of Systems and Control Engineering, Tokyo Institute of Technology, Tokyo 152-8552, Japan
* Author to whom any correspondence should be addressed.

E-mail: kato.y.bg@m.titech.ac.jp

Keywords: synchronization, nonlinear dynamics, open quantum systems, quantum synchronization

Abstract

We study synchronization of a quantum van der Pol oscillator with a harmonic drive and demonstrate that quantum synchronization can be enhanced by performing continuous homodyne measurement on an additional bath linearly coupled to the oscillator and applying feedback control to the oscillator. The phase coherence of the oscillator is increased by reducing quantum fluctuations via the continuous measurement, whereas the measurement backaction inevitably induces fluctuations around the phase-locking point. We propose a simple feedback policy for suppressing measurement-induced fluctuations by adjusting the frequency of the harmonic drive, which results in enhancement of quantum synchronization. We further demonstrate that the maximum enhancement of quantum synchronization is achieved by performing quantum measurement on the quadrature angle at which the phase diffusion of the oscillator is the largest and the maximal information on the oscillator phase is extracted.

1. Introduction

Studies pertaining to synchronization of nonlinear oscillators began in the 17th century when Huygens first documented the discovery of mutual synchronization between two pendulum clocks. Henceforth, synchronization phenomena have been widely observed in various fields of science and technology, e.g. laser oscillations, chemical oscillations, spiking neurons, chorusing crickets, and mechanical vibrations [1–5]. Furthermore, synchronization have also been analyzed in engineering applications, such as voltage standards [6], injection locking [7], phase-locked loops in electrical circuits [8], and deep brain stimulation for the treatment of Parkinson's disease [9].

Experimental studies of synchronizing nonlinear oscillators have recently reached the micrometer and nanometer scales, including micro- and nanomechanical oscillators [10–17], microlasers [18], and spin-torque oscillators [19], and experimental demonstrations of quantum phase synchronization in spin-1 atoms [20] and on the IBM Q system [21] have been reported. Owing to such experimental developments, the theoretical analysis of quantum synchronization has received significant attention. For example, synchronization of a quantum van der Pol (vdP) oscillator with harmonic drive [22–28] and squeezing [29], synchronization of coupled quantum vdP oscillators [30–33], quantum spin systems [34, 35], optomechanical systems [36–38], ensembles of atoms [39, 40], and isolated quantum systems [41], quantum chimera states [42], quantum synchronization blockade [43], and probing quantum synchronization using spin correlations [44] have been studied theoretically. These studies have revealed that quantum fluctuations generally induce phase diffusion in quantum limit-cycle oscillators and disturb strict synchronization [22–24, 29, 30]. To overcome this deleterious effect of quantum fluctuations on synchronization, Sonar *et al* studied the effect of squeezing and demonstrated that the entrainment of a quantum vdP oscillator to a squeezing signal can suppress quantum fluctuations and consequently enhance quantum synchronization [29].

Measurement is one of the peculiar features in quantum systems; it changes the quantum state of a system depending on the probabilistic outcomes [45, 46]. When knowledge about a system is indirectly

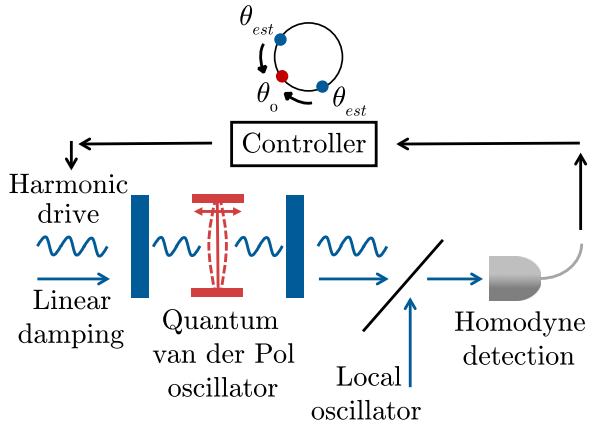

Figure 1. Enhancement of synchronization of a quantum vdP oscillator with a harmonic drive via the continuous homodyne measurement and feedback control.

obtained by continuously monitoring the output of a field environment interacting with an open quantum system, the system dynamics under the measurement can be described by a continuous quantum trajectory, i.e. a stochastic evolution of the system conditioned by the measurement outcomes [47, 48]. This continuous measurement framework facilitates the investigation of novel dynamical features of quantum measurement, such as state preparation [49, 50], dynamical creation of entanglement [51], and unveiling [52, 53] and controlling [54] of the chaotic behavior of quantum systems. It is also notable that the experimental realization of continuous measurement has been investigated recently [55–57].

Furthermore, the effect of continuous measurement of quantum limit-cycle oscillators has also been investigated, such as measurement-induced transitions between in-phase and anti-phase quantum synchronization [37], enhancement of nonclassicality in optomechanical oscillators via measurement [58], improvement in accuracy of Ramsey spectroscopy through measurement of synchronized atoms [40], characterization of synchronization using quantum trajectories [32], realization of quantum relaxation oscillators [59], and instantaneous quantum phase synchronization of two decoupled quantum limit-cycle oscillators induced by conditional photon detection [60]. However, to the best of our knowledge, the effect of continuous measurement on the enhancement of quantum synchronization has never been discussed.

In this study, we consider synchronization of a quantum vdP oscillator with a harmonic drive and demonstrate that performing continuous homodyne measurement on an additional bath linearly coupled to the oscillator and applying a feedback control to the oscillator can enhance quantum synchronization. We demonstrate that quantum fluctuations disturbing the phase coherence can be reduced by continuous homodyne measurement, and that the measurement backaction inevitably induces stochastic deviations from the phase-locking point. We propose a simple feedback policy that can suppress the fluctuations by adjusting the frequency of the harmonic drive. Furthermore, we demonstrate that the maximal enhancement of quantum synchronization can be achieved by performing the measurement on the quadrature angle at which the phase diffusion of the oscillator is the largest and the maximal information on the phase of the oscillator can be obtained via the measurement. It is shown that, by using continuous measurement and feedback control, more significant enhancement of phase coherence can be achieved than simply optimizing the waveform of the periodic amplitude modulation of the driving signal in the feed-forward setting as analyzed in our previous study [25].

2. Model

We consider a quantum vdP oscillator [22, 23] subjected to a harmonic drive. A schematic diagram of the physical setup is shown in figure 1. We further introduce an additional linear bath coupled to the oscillator, perform continuous homodyne measurement of the output field from the oscillator to the bath, and apply a feedback control to adjust the frequency of the harmonic drive (figure 1). The quantum vdP model is derived by considering a harmonic oscillator (main system) linearly and nonlinearly coupled to environmental baths and tracing out the environmental degrees of freedom. It is commonly assumed that baths have large degrees of freedom and the correlation times of the baths are significantly shorter than the timescale of the main system. The Markovian approximation of the baths can then be employed to derive the reduced master equation in the Lindblad form describing the main system under the effect of linear and nonlinear dissipation, yielding the quantum vdP model [22, 61].

We denote by ω_0 and ω_d the frequencies of the quantum vdP oscillator and harmonic drive, respectively. The stochastic master equation of the quantum system in the coordinate frame rotating with the frequency ω_d is written as [22–24]

$$\begin{aligned} d\rho &= \{-i\left[-(\Delta+\Delta_{fb})a^\dagger a + iE(a-a^\dagger),\rho\right] + \gamma_1\mathcal{D}[a^\dagger]\rho + \gamma_2\mathcal{D}[a^2]\rho \\ &\quad + \gamma_3\mathcal{D}[a]\rho\}\,dt + \sqrt{\eta\gamma_3}\mathcal{H}[a\,e^{-i\theta}]\rho dW, \\ dY &= \sqrt{\eta\gamma_3}\,\mathrm{Tr}[(a\,e^{-i\theta} + a^\dagger\,e^{i\theta})\rho]dt + dW, \end{aligned} \tag{1}$$

with $\mathcal{D}[L]\rho = L\rho L^\dagger - \frac{1}{2}(L^\dagger L\rho + \rho L^\dagger L)$, $\mathcal{H}[L]\rho = L\rho + \rho L^\dagger - \mathrm{Tr}[(L+L^\dagger)\rho]\rho$, where $\mathcal{D}$ is the Lindblad form and $\mathcal{H}[a\,e^{-i\theta}]$ characterizes the measurement on the quadrature $ae^{-i\theta} + a^\dagger e^{i\theta}$, ρ is the density matrix representing the system state, a and $a^\dagger$ denote the annihilation and creation operators ($\dagger$ represents Hermitian conjugate), respectively, $\Delta = \omega_d - \omega_0$ is the frequency detuning of the harmonic drive from the oscillator, Δ_{fb} is the feedback control to adjust the frequency detuning, i.e. the frequency of the harmonic drive, E is the intensity of the harmonic drive, γ_1, γ_2, and γ_3 represent the decay rates for the negative damping, nonlinear damping, and linear damping, respectively, η is the efficiency of the measurement (we set $\eta = 1$ when the measurement is performed, and $\eta = 0$ when it is not), θ specifies the quadrature angle of the measurement, W represents a Wiener process satisfying $\mathbb{E}[dW] = 0$ and $\mathbb{E}[dW^2] = dt$, Y is the output of the measurement result, and the reduced Planck's constant is set as $\hbar = 1$.

In the following, we use the parameter settings such that the oscillator is synchronized with the harmonic drive and the Wigner distribution [61] of the steady-state density matrix ρ_{ss} of equation (1) is concentrated around a stable phase-locking point along the limit-cycle orbit in the classical limit (see, e.g. figure 3(a)) when the measurement is not performed ($\eta = 0$).

We set the feedback control Δ_{fb} as (see appendix A for details)

$$\Delta_{fb} = -K_{fb}(\theta_{est} - \theta_0), \tag{2}$$

where $K_{fb}(>0)$ represents the feedback gain and $\theta_0 = \arctan\left(\mathrm{Tr}[p\rho_{ss}]/\mathrm{Tr}[x\rho_{ss}]\right)$ represents the locking phase in the absence of the measurement, which is calculated as the angle between the expectation values of the position operator $x = (a+a^\dagger)/2$ and the momentum operator $p = -i(a-a^\dagger)/2$ with respect to the steady-state ρ_{ss} of equation (1) without measurement, and $\theta_{est} = \arctan\left(\mathrm{Tr}[p\rho_{est}]/\mathrm{Tr}[x\rho_{est}]\right)$, which is chosen such that $-\pi + \theta_0 \leqslant \theta_{est} < \theta_0 + \pi$, represents the phase of the system calculated from the instantaneous state ρ_{est} of equation (1) with measurement conditioned on the measurement record. The feedback control above can actually suppress the fluctuations of the system state around the phase-locking point as will be shown in the next section.

Note that we cannot introduce the feedback control without the linear bath in the present scheme because the continuous measurement should be performed on the linear bath coupled to the main system. Also, since we introduce the feedback control in the frequency detuning, the instantaneous frequency of the driving signal varies (when the natural frequency of the vdP oscillator is fixed). It is assumed that this variation in the driving frequency due to the feedback control is much smaller than the frequencies ω_0 and ω_d and, when the feedback control works and the synchronized state is maintained, the driving frequency remains approximately constant on average and the vdP oscillator is entrained to this frequency.

To evaluate the phase coherence of the quantum vdP oscillator, we use the order parameter [27, 37]

$$S_1 = |S_1|\,e^{i\phi_1} = \frac{\mathrm{Tr}[a\rho]}{\sqrt{\mathrm{Tr}[a^\dagger a\rho]}}, \tag{3}$$

which is a quantum analog of the order parameter for a single classical noisy oscillator [2, 3]. The absolute value $|S_1|$ quantifies the degree of phase coherence and assumes the values in $0 \leqslant |S_1| \leqslant 1$, where $|S_1| = 1$ when the oscillator state is perfectly phase-coherent and $|S_1| = 0$ when the state is perfectly phase-incoherent. Here ϕ_1 represents the average phase value of the oscillator.

3. Results

Numerical simulations of equation (1) are performed. In sections 3.1–3.3, we set the parameter values in the semiclassical regime, $(\Delta, \gamma_2, \gamma_3, E)/\gamma_1 = (0.05, 0.05, 0.1, \sqrt{0.1})$, to clarify the relation between the quantum system and its classical limit [24], and the feedback gain is set as $K_{fb}/\gamma_1 = 1$ when we apply the feedback control. In section 3.4, we discuss the applicability of the proposed scheme in the quantum regime with parameter values $(\Delta, \gamma_2, \gamma_3, E)/\gamma_1 = (0.05, 0.25, 0.25, \sqrt{0.1})$, and apply feedback control with a feedback gain $K_{fb}/\gamma_1 = 7.5$. In sections 3.1, 3.2, and 3.4, we set $\theta = 0$ for the quadrature of measurement

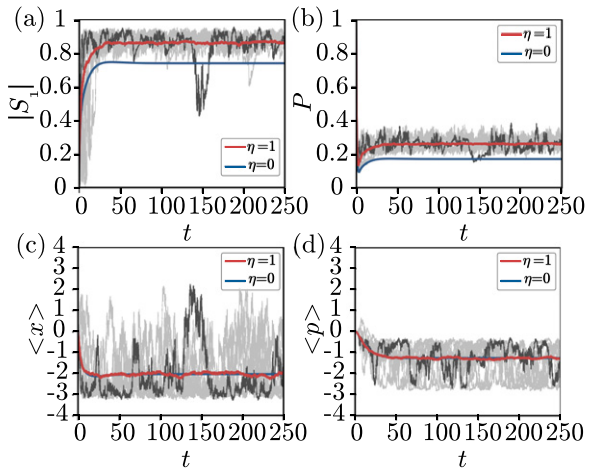

Figure 2. Measurement-induced increase in phase coherence without feedback control in semiclassical regime. (a) Order parameter $|S_1|$. (b) Purity P. (c) Expectation values of position operator $\langle x \rangle$. (d) Expectation values of momentum operator $\langle p \rangle$. For the case with measurement ($\eta = 1$), average values of results calculated from 300 trajectories are shown by red lines and 10 out of 300 individual trajectories are shown by gray lines, with the dark one representing a single realization of the trajectory. For the case without measurement ($\eta = 0$), the results of a single trajectory are shown by blue lines.

and, in section 3.3, the effect of varying θ is analyzed. We always set the initial state of the simulation as the vacuum state, i.e. $\rho = |0\rangle\langle 0|$.

3.1. Without feedback control

We first consider the case without feedback control, i.e. $K_{\mathrm{fb}} = 0$, in the semiclassical regime. In the case with measurement, we calculated the average values over 300 trajectories obtained by the numerical simulations of equation (1) from the same initial state ($\rho = |0\rangle\langle 0|$) because the system trajectories behave stochastically. The average results are compared with the results in the case without measurement, where the system trajectory of equation (1) is deterministic.

Figures 2(a)–(d) show the trajectories of the absolute values of the order parameter $|S_1|$ quantifying the degree of phase coherence, the purity $P = \mathrm{Tr}[\rho^2]$, the expectation value of the position operator $\langle x \rangle = \mathrm{Tr}[x\rho]$, and the expectation value of the momentum operator $\langle p \rangle = \mathrm{Tr}[p\rho]$, respectively. Note that these expectation values are fluctuating in the case with measurement.

As shown in figure 2(a), the average values of the order parameter $|S_1|$ with measurement are larger than the (deterministic) value of $|S_1|$ without measurement, e.g. $|S_1| = 0.859$ with measurement and $|S_1| = 0.737$ without measurement at $t = 250$, signifying the phase coherence increased on average due to the continuous homodyne measurement. The increase in the purity is evident in figure 2(b); the average values of the purity P with measurement are larger than the stationary value of P without measurement, e.g. $P = 0.258$ with measurement and $P = 0.169$ without measurement at $t = 250$ sufficiently after the initial relaxation.

We note that the observed increase in $|S_1|$ or P is an average effect; the values of these quantities for a single trajectory of equation (1) with the measurement fluctuates significantly and occasionally take smaller values than those without measurement, as shown by the dark gray lines in figures 2(a) and (b). We also note that the increase in the purity implies the reduction in the phase diffusion of the oscillator (see appendix B). In association with the increase in phase coherence by the measurement, the measurement backaction inevitably induces fluctuations in the system state around the phase-locking point. This is evident from figures 2(c) and (d), which show 10 trajectories of $\langle x \rangle$ and $\langle p \rangle$ obtained by simulating equation (1) with measurement (gray lines) exhibit strong fluctuations.

The increase in phase coherence by the measurement is also observed in the Wigner distribution. Figure 3(a) shows the steady-state Wigner distribution obtained from equation (1) without measurement (ρ converges to a steady state in this case), and figures 3(b)–(d) show the instantaneous Wigner distributions at $t = 250$ of three trajectories obtained by simulating equation (1) with measurement (ρ behaves stochastically in this case).

Comparing figures 3(b)–(d) with figure 3(a), we observe increase in phase coherence by the continuous homodyne measurement from the strongly concentrated Wigner distributions. We also observe that the location of the distribution differs by trajectory because the measurement backaction randomly disturbs the system state based on the measurement outcomes. We here note that the increase in the phase coherence of the Wigner distribution occurs for each stochastic realization of the stochastic master equation (1) with

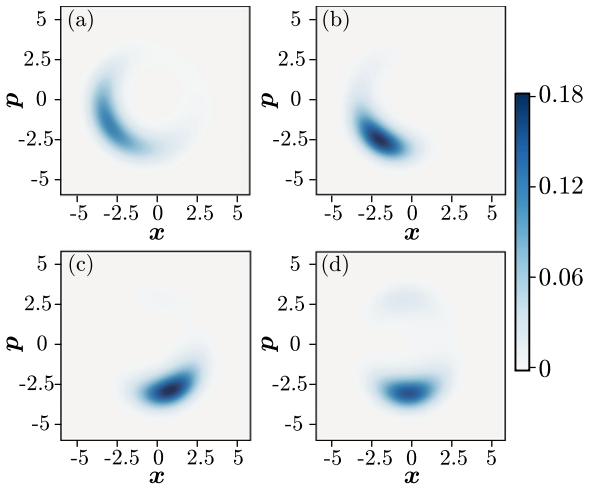

Figure 3. Wigner distributions of system without feedback control in semiclassical regime. (a) Wigner distribution of steady state of equation (1) without measurement. (b)–(d) Wigner distributions of three different trajectories of equation (1) with measurement at $t = 250$.

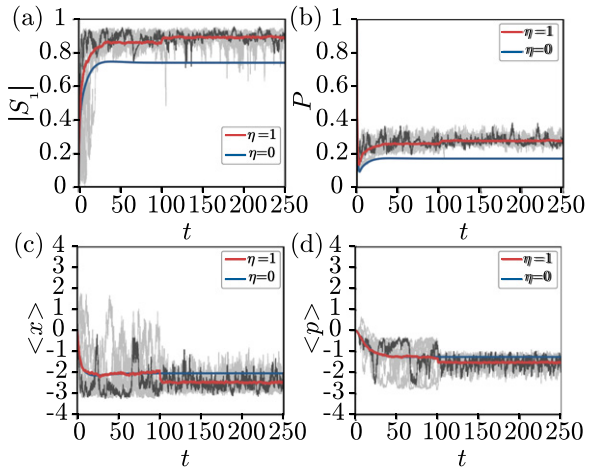

Figure 4. Measurement-induced enhancement of quantum synchronization with feedback control in semiclassical regime. Feedback control is applied from $t = 100$. (a) Order parameter $|S_1|$. (b) Purity P. (c) Expectation values of the position operator $\langle x \rangle$. (d) Expectation values of the momentum operator $\langle p \rangle$. For the case with measurement ($\eta = 1$), average values of results calculated from 300 trajectories are shown by red lines and 10 out of 300 individual trajectories are shown by gray lines with the dark one representing a single realization of the trajectory. For the case without measurement ($\eta = 0$), the results of a single trajectory are shown by blue lines.

measurement. If we average the Wigner distributions with measurement over all realizations, the result without measurement as shown in figure 3(a) is obtained.

3.2. With feedback control

As presented in section 3.1, we observed that the measurement increases phase coherence but induces fluctuations in the system state around the phase-locking point simultaneously. To suppress the fluctuations of the system state, we introduce the feedback control expressed in equation (2).

Figures 4(a)–(d) show the trajectories of $|S_1|$, P, $\langle x \rangle$, and $\langle p \rangle$, respectively. The feedback control is applied from $t = 100$. As shown in figure 4(a), the average order parameter $|S_1|$ with measurement takes larger values than $|S_1|$ without measurement, e.g. $|S_1| = 0.889$ with measurement and $|S_1| = 0.737$ without measurement at $t = 250$. We also see in figure 4(b) that the average values of P with measurement are larger than those without measurement, e.g. $P = 0.275$ with measurement and $P = 0.169$ without measurement at $t = 250$.

The role of the feedback control is evident from figures 4(c) and (d), where 10 trajectories of $\langle x \rangle$ and $\langle p \rangle$ obtained by simulating equation (1) with measurement are shown (gray lines). The fluctuations around the phase-locking point are suppressed by the feedback control that is turned on after $t = 100$. We note that we

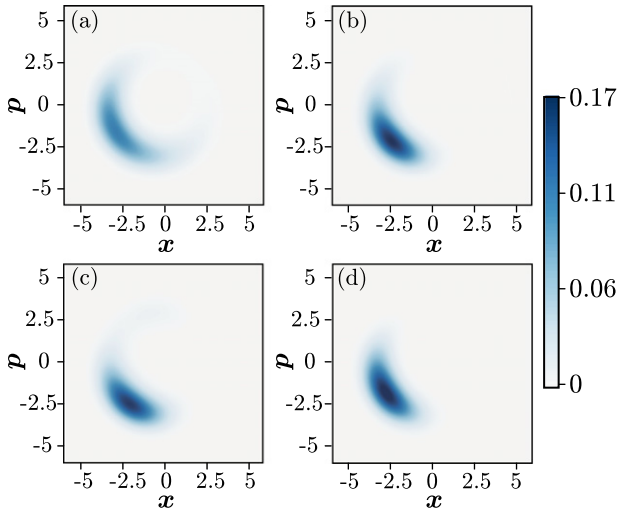

Figure 5. Wigner distributions of system with feedback control in semiclassical regime. (a) Wigner distribution of steady state of equation (1) without measurement. (b)–(d) Wigner distributions of three different trajectories of equation (1) with measurement at $t = 250$. Feedback control is applied from time $t = 100$.

used the same sequences of the Wiener increments in the numerical simulations of equation (1) in the case without feedback control.

The average values of $\langle x\rangle$ and $\langle p\rangle$ (red lines) are smaller than those for the case without measurement (blue lines). This can be explained as follows. The backaction induces strong fluctuations in $\langle x\rangle$. Without feedback control, $\langle x\rangle$, which fluctuates near the phase-locking point, occasionally exhibits a large increase along the limit-cycle trajectory to the clockwise direction. This large increase in $\langle x\rangle$ is suppressed by the feedback control, which results in a smaller average value of $\langle x\rangle$. Although the backaction is weaker for $\langle p\rangle$, the suppression of large increase in $\langle x\rangle$ by the feedback control results in a smaller average value of $\langle p\rangle$.

The effect of feedback control for suppressing the fluctuations of the system state is also evident from the Wigner distribution of the system. Figure 5(a) shows the steady-state Wigner distribution of equation (1) without measurement, whereas figures 5(b)–(d) show three realizations of the Wigner distributions at $t = 250$ of equation (1) with measurement. Comparing figures 5(b)–(d) with figures 3(b)–(d), it is clear that the fluctuations around the phase-locking point are suppressed effectively by the feedback control.

The results above indicate that enhancement of synchronization, i.e. larger phase coherence and smaller fluctuations around the phase-locking point, can be achieved via continuous measurement and feedback control.

3.3. Dependence on measurement quadrature

Thus far, we have fixed θ, the quadrature of the measurement, at 0. Next, we consider the effect of varying θ on the enhancement of quantum synchronization.

Figures 6(a) and (b) show the average values of $|S_1|$ and P at $t = 250$ for $0 \leqslant \theta \leqslant 2\pi$, respectively, which are calculated from 400 trajectories of equation (1) with measurement and the feedback control. For comparison, we also show the values of $|S_1|$ and P for the steady state of equation (1) without the measurement. The maximum values of $|S_1|$ and P are achieved at $\theta = 2.199$, which is approximately orthogonal to the locking phase, i.e. $\theta_0 = 3.696$.

The result above can be interpreted as follows. The phase diffusion of the oscillator is maximized when θ is orthogonal to θ_0, and performing the measurement on the quadrature specified by this θ extracts the maximum information on the oscillator phase. Hence, the maximum reduction in quantum fluctuations and enhancement in synchronization are attained at the above quadrature angle. Note that uncertainty in the oscillator phase always exists due to quantum fluctuations and no matter which quadrature angle we choose, we can obtain non-zero information about the oscillator phase and enhance quantum synchronization via the continuous measurement.

3.4. Applicability in stronger quantum regime

Finally, we discuss the enhancement of quantum synchronization via continuous measurement and feedback control in a stronger quantum regime. The parameters are shown at the beginning of section 3.

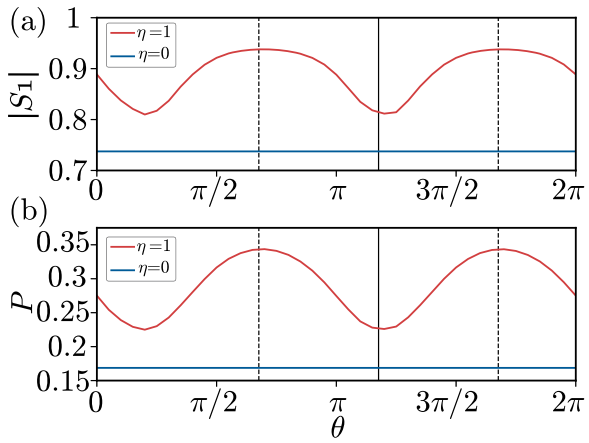

Figure 6. Dependence of results on measurement quadrature. (a) Order parameter $|S_1|$. (b) Purity P. Order parameter and purity averaged over 400 trajectories with measurement at $t = 250$ (red lines) are compared with those for a single trajectory without measurement (blue lines). Phase-locking point θ_0 (a solid black vertical line) and points orthogonal to the phase-locking point $\theta_0 + \pi/2$ (dotted black vertical lines) are shown.

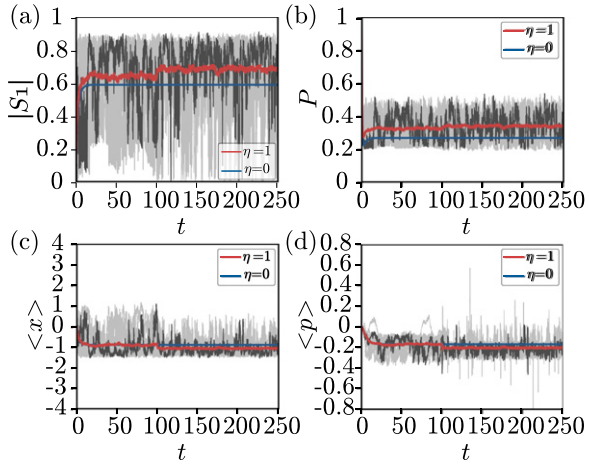

Figure 7. Measurement-induced enhancement of quantum synchronization with feedback control in quantum regime. Feedback control is applied from $t = 100$. (a) Order parameter $|S_1|$. (b) Purity P. (c) Expectation values of position operator $\langle x \rangle$. (d) Expectation values of momentum operator $\langle p \rangle$. For the case with measurement ($\eta = 1$), averaged values of results calculated from 300 trajectories are shown by red lines, and 10 out of 300 individual trajectories are shown by gray lines with the dark one representing a single realization of the trajectory. For the case without measurement ($\eta = 0$), results of a single trajectory are shown by blue lines.

Figures 7(a)–(d) show the trajectories of $|S_1|$, P, $\langle x \rangle$, and $\langle p \rangle$, respectively. The feedback control is applied after $t = 100$.

As shown in figure 7(a), the average order parameter $|S_1|$ with measurement takes larger values than $|S_1|$ without measurement, e.g. $|S_1| = 0.683$ with measurement and $|S_1| = 0.586$ without measurement at $t = 250$. We also see in figure 7(b) that the averaged values of P with measurement are larger than the values of P without measurement, e.g. $P = 0.338$ with measurement and $P = 0.266$ without measurement at $t = 250$.

As shown from the results above, both $|S_1|$ and P increase on average with measurement even in this quantum regime. The suppression of the measurement-induced fluctuations by the feedback control is shown in figure 7(c), where 10 trajectories of $\langle x \rangle$ obtained by simulating equation (1) with measurement are shown (gray lines). We see that the fluctuations in $\langle x \rangle$ around the phase-locking point are suppressed by the feedback control which is turned on after $t = 100$. However, in figure 7(d) where 10 trajectories of $\langle p \rangle$ obtained by simulating equation (1) with measurement are shown (gray lines), the fluctuations in $\langle p \rangle$ still remain and can be even stronger after the feedback control is turned on at $t = 100$. We note that the fluctuations in $\langle p \rangle$ become smaller on average but $\langle p \rangle$ also exhibits occasional bursty increases when the feedback control is applied. This is because the feedback control induces more localized states with stronger

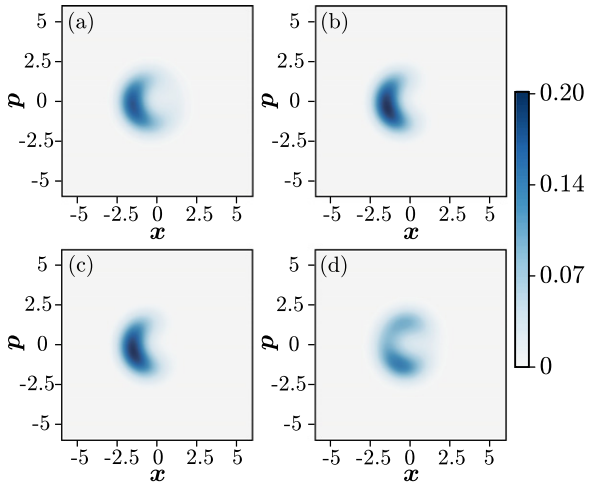

Figure 8. Wigner distributions of system with feedback control in quantum regime. (a) Wigner distribution of steady state of equation (1) without measurement. (b)–(d) Wigner distributions of three different trajectories of equation (1) with measurement at $t = 250$. Feedback control is applied from time $t = 100$.

phase coherence than the case without feedback and measurement-induced fluctuations of such states yield larger variations in $\langle p \rangle$.

These results are also observed from the Wigner distribution of the system. Figure 8(a) shows the steady-state Wigner distribution of equation (1) without measurement and figures 8(b)–(d) show three realizations of the Wigner distributions at $t = 250$ of equation (1) with measurement, respectively. The fluctuations around the phase-locking point are suppressed effectively by the feedback control and the enhancement of quantum synchronization is achieved in figures 8(b) and (c). However, the measurement-induced fluctuation still remains and the system occasionally exhibits transient short-time failures of synchronization with low phase coherence as shown in figure 8(d).

The numerical results shown in figures 7 and 8 indicate that quantum synchronization is enhanced only probabilistically in the strong quantum regime considered here. We repeated numerical simulations from the same initial condition and empirically obtained a success rate of approximately 80 percent for the enhancement of quantum synchronization, namely, Wigner distributions at time $t = 250$ are strongly localized around the phase-locking point θ_0 for approximately 80 percent of the trajectories. Thus, in this regime, because of the strong quantum fluctuations, the feedback control occasionally fails to suppress the measurement-induced fluctuations and enhance quantum synchronization. We note here that, because the feedback signal is different for each trajectory, the Wigner distribution is not averaged over trajectories but its individual realizations for different trajectories are plotted in figures 5 and 8.

We also note that the strong quantum fluctuations lead to the weaker enhancement of synchronization. This is evident in the improvement of $|S_1| = 0.683$ from $|S_1| = 0.586$ by a factor $0.683/0.586 = 1.166$ in the quantum regime, which is smaller than the improvement of $|S_1| = 0.889$ from $|S_1| = 0.737$ by a factor $0.889/0.737 = 1.206$ in the semiclassical regime in figures 4 and 5. More detailed and systematic numerical analysis in the strong quantum regime and finding an improved feedback strategy for achieving the enhancement of quantum synchronization to minimize the probability of failure as shown in figure 8(d) are the subject of future study.

4. Discussion

We have confirmed that our scheme can enhance synchronization of the vdP oscillator to the harmonic drive. Here we discuss several perspectives for future studies.

(a) Though not treated in this study, the effect of thermal noise [61] and measurement inefficiency [48] should be taken into account to consider more realistic experimental situations. If we consider these effects, the intensities of the feedback signal and the noise term in the model will change. However, it is expected that, as long as their effects are not too strong, the qualitative behavior of the system will not change and enhancement of synchronization will occur because the essential mechanism of the scheme explained in the appendices remains unchanged.

(b) We focused only on the synchronized regime and tried to improve the coherence by using continuous measurement and feedback. The effect of continuous measurement on the overall synchronization

property in a wider frequency range, in particular, Arnold's tongue [27, 30], is of great importance. For example, it is expected that the shape of Arnold's tongue can considerably change depending on the measurement inefficiency. This phenomenon will be studied in detail in our future work.

(c) In this study, we introduced the feedback control in the frequency of the external drive for suppressing measurement-induced fluctuations. Alternatively, we may adjust the quadrature of the harmonic drive based on the measurement outcomes to enhance synchronization without changing the frequency of the external drive. The well-known Markovian feedback [48] may also be useful for enhancing quantum synchronization. Apart from the feedback strategy, an additional linear-damping bath without measurement also enhances synchronization of a quantum vdP oscillator with an external drive in the deep quantum regime as discussed in reference [62].

(d) It is interesting to investigate the connection between enhancement of phase coherence by measurement and uncertainty relation. The measurement plays two conflicting roles on synchronization: (i) enhancing the coherence by information gain (the term $\mathcal{H}[a\,\mathrm{e}^{-\mathrm{i}\theta}]$ in equation (1)) and (ii) destroying the locking to the harmonic forcing by the disturbance (the term $\mathcal{D}[a]$ in equation (1)) [63]. The dependence of the result on the optimal quadrature angle of the measurement is also related to the uncertainty principle. A more detailed analysis on this point would provide insights into how the uncertainty relation affects the enhancement of quantum synchronization.

(e) It would also be important to perform a systematic analysis of the transition from the semiclassical regime to the quantum regime and analyze the performance of our feedback control in enhancing synchronization, which will clarify the applicability of our scheme in the strong quantum regime.

(f) Studying the enhancement of quantum synchronization of a quantum vdP oscillator with squeezing drive [29] by using the present scheme would also be interesting, because it is expected that the combining effects of enhancement of quantum synchronization via squeezing lights and our scheme of continuous measurement and feedback control would be useful for further enhancement of quantum synchronization.

5. Conclusion

We considered synchronization of a quantum vdP oscillator with a harmonic drive. We demonstrated that introducing an additional linear bath coupled to the system and performing continuous homodyne measurement of the bath can increase the phase coherence of the system. We also proposed a simple feedback policy for suppressing the fluctuations in the system state around the phase-locking point by adjusting the frequency of the harmonic drive, and achieved the measurement-induced enhancement of synchronization. We further demonstrated that the maximum enhancement of synchronization is achieved when we perform measurement on the quadrature angle at which the phase diffusion of the oscillator is maximized and the maximum information regarding the oscillator phase is attained. Finally, we demonstrated that the enhancement of quantum synchronization via continuous measurement and feedback control can be achieved with a high probability of success even in the stronger quantum regime.

The proposed system can, in principle, be implemented using the current experimental setups; synchronization of a quantum vdP with a harmonic drive can be experimentally implemented using optomechanical systems [23] or ion traps [22], and the feedback control can be implemented by adjusting the frequency of the harmonic drive using the measurement outcomes. Quantum measurement, an essential feature in quantum systems, can thus help us resolve the issue of quantum fluctuations that disturb strict quantum synchronization and will be important for the realization and future applications of quantum synchronization in the evolving field of quantum technologies.

Acknowledgments

Numerical simulations are performed using the QuTiP numerical toolbox [64]. The authors gratefully thank N Yamamoto for the stimulating discussions. We acknowledge JSPS KAKENHI JP17H03279, JP18H03287, JPJSBP120202201, JP20J13778, and JST CREST JP-MJCR1913 for financial support.

Appendix A. Feedback policy

We discuss the feedback policy for suppressing measurement-induced fluctuations around the phase-locking point. To understand the core idea of the feedback policy with a simple model, we consider the system described in equation (1) without the linear coupling to the bath, i.e. $\gamma_3 = 0$. We also assume

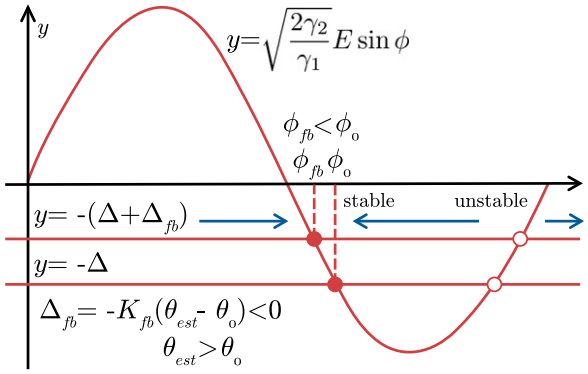

Figure 9. Schematic diagram of feedback policy for suppressing fluctuations around phase-locking point. Feedback control shifts phase-locking point from ϕ_0 to $\phi_{\rm fb}$ that is opposite to the direction from θ_0 to $\theta_{\rm est}$.

that the system is in the semiclassical regime and the oscillator dynamics can be described by a semiclassical stochastic differential equation (SDE) whose deterministic part possesses a stable limit-cycle solution. We can then apply the semiclassical phase reduction [24] to obtain an approximate one-dimensional SDE for the phase variable of the oscillator and use the standard classical methods for the phase equation [1–5] to analyze synchronization dynamics of the oscillator driven by a periodic forcing.

When the quantum noise is sufficiently weak and the classical limit can be taken, the deterministic phase equation for the oscillator is expressed as (see also the next section) [23, 24]

$$\frac{\mathrm{d}\phi}{\mathrm{d}t} = \Delta + \Delta_{\rm fb} + \sqrt{\frac{2\gamma_2}{\gamma_1}}E\,\sin\,\phi. \tag{A1}$$

When $|\Delta+\Delta_{\rm fb}| \leqslant \sqrt{\frac{2\gamma_2}{\gamma_1}}E$, there exists a stable fixed point of equation (A1), which corresponds to the phase-locking point of the system with the harmonic driving signal under the feedback control, satisfying

$$\phi_{\rm fb} = -\arcsin\left(\frac{\Delta+\Delta_{\rm fb}}{E}\sqrt{\frac{\gamma_1}{2\gamma_2}}\right). \tag{A2}$$

The fixed point when the feedback control is turned off, i.e. $\Delta_{\rm fb}=0$, is expressed as

$$\phi_0 = -\arcsin\left(\frac{\Delta}{E}\sqrt{\frac{\gamma_1}{2\gamma_2}}\right). \tag{A3}$$

Figure 9 shows a schematic diagram of the feedback policy for suppressing fluctuations around the phase-locking point. As shown in figure 9, when $\theta_{\rm est}>\theta_0$, the feedback control is $\Delta_{\rm fb}=-K_{\rm fb}(\theta_{\rm est}-\theta_0)<0$ and hence $\phi_{\rm fb}<\phi_0$. Similarly, when $\theta_{\rm est}<\theta_0$, we obtain $\phi_{\rm fb}>\phi_0$. Therefore, the feedback control shifts the locking phase from ϕ_0 to $\phi_{\rm fb}$, which is opposite to the direction from θ_0 to $\theta_{\rm est}$, and is expected to suppress the fluctuations of the system around the phase-locking point.

Appendix B. Relationship between the phase diffusion and purity

We discuss the relation between the phase diffusion and purity of the quantum vdP oscillator when the measurement is absent. We consider the system described in equation (1) without the linear coupling to the bath, i.e. $\gamma_3=0$; additionally, we assume that the system is in the semiclassical regime and driven by the weak perturbation. The system can then be approximately described by a SDE of the phase variable of the oscillator by using the semiclassical phase reduction theory [24].

We introduce the following rescaled quantities: $\gamma_2=\sigma\gamma_1\gamma_2', \Delta+\Delta_{\rm fb}=\gamma_1(\Delta'+\Delta_{\rm fb}'), E=\epsilon\gamma_1E'/\sqrt{\sigma}, \mathrm{d}t'=\gamma_1\mathrm{d}t, \mathrm{d}W'=\sqrt{\gamma_1}\mathrm{d}W$ with dimensionless parameters γ_2', Δ', $\Delta_{\rm fb}'$, and E' of $\mathcal{O}(1)$. We set $0<\sigma\ll 1$ (the system is in the semiclassical regime) and $0<\epsilon\ll 1$ (the perturbation is weak). The corresponding semiclassical phase equation for the quantum system in equation (1) is then given by [24]

$$\mathrm{d}\phi = \left(\Delta'+\Delta_{\rm fb}'+\epsilon\sqrt{2\gamma_2'}E'\,\sin\,\phi\right)\mathrm{d}t' + \sqrt{\sigma D_0}\mathrm{d}W', \tag{B1}$$

with $D_0=\frac{3\gamma_2'}{2}$.

We first evaluate the phase diffusion of the oscillator based on the effective diffusion constant of equation (B1) [65],

$$D_{\rm eff} \propto \frac{1}{(\langle \exp(v(\phi)/(\sigma D_0))\rangle_\phi \langle \exp(-v(\phi)/(\sigma D_0))\rangle_\phi)}, \tag{B2}$$

where the potential $v(\phi)$ is given by $v(\phi) = -\int_{\phi_0}^{\phi} (\Delta' + \Delta'_{\rm fb} + \epsilon\sqrt{2\gamma'_2}E' \sin\phi')\mathrm{d}\phi'$ with a reference phase point ϕ_0 and $\langle\cdot\rangle_\phi = \frac{1}{2\pi}\int_0^{2\pi}(\cdot)\mathrm{d}\phi$. When σ is sufficiently small, using the saddle-point approximation $\langle \exp(v(\phi)/(\sigma D_0))\rangle_\phi \approx \exp(v_{\max}/(\sigma D_0))$ and $\langle \exp(-v(\phi)/(\sigma D_0))\rangle_\phi \approx \exp(-v_{\min}/(\sigma D_0))$, the effective diffusion constant can be approximated as

$$D_{\rm eff} \approx \frac{1}{\exp((v_{\max} - v_{\min})/(\sigma D_0))}, \tag{B3}$$

where $v_{\max}$ and $v_{\min}$ are the maximum and minimum values of the potential $v(\phi)$, respectively (see [66] for details), and the constant factors are omitted.

We next evaluate the purity. Using semiclassical phase reduction theory [24], the density matrix can be approximately reconstructed from the phase equation as $\rho \approx \int_0^{2\pi} \mathrm{d}\phi P(\phi)\,|\alpha_0(\phi)\rangle\,\langle\alpha_0(\phi)|$, where $\alpha_0(\phi) = \sqrt{\frac{1}{2\sigma\gamma'_2}}\exp(\mathrm{i}\phi)$ is the system state at ϕ on the classical limit cycle in the phase space of the P representation [61] and $P(\phi)$ is the steady-state probability distribution of the Fokker–Planck equation for the phase variable given by ([3], chapter 9)

$$P(\phi) \propto \int_0^{2\pi} \mathrm{d}\phi' \exp\left[\frac{2(v(\phi'+\phi) - v(\phi))}{\sigma D_0}\right]. \tag{B4}$$

Because the size of the limit cycle is $O(1/\sqrt{\sigma})$, i.e. $\alpha_0(\phi) = O(1/\sqrt{\sigma})$, when σ is sufficiently small, the purity can be evaluated by using saddle-point approximation as

$$\begin{aligned} P = \mathrm{Tr}(\rho^2) &\approx \int_0^{2\pi}\mathrm{d}\phi P(\phi)\int_0^{2\pi}\mathrm{d}\phi' P(\phi')\exp(-|\alpha_0(\phi)-\alpha_0(\phi')|^2) \\ &\approx \int_0^{2\pi}\mathrm{d}\phi P^2(\phi) \approx \int_0^{2\pi}\mathrm{d}\phi\left(\int_0^{2\pi}\mathrm{d}\phi' \exp\left[\frac{2(v(\phi'+\phi)-v(\phi))}{\sigma D_0}\right]\right)^2 \\ &\approx \int_0^{2\pi}\mathrm{d}\phi\left(\exp\left[\frac{2(v_{\max}-v(\phi))}{\sigma D_0}\right]\right)^2 \approx \exp\left[\frac{4(v_{\max}-v_{\min})}{\sigma D_0}\right], \end{aligned}$$

where the constant factors are omitted. The effective diffusion constant $D_{\rm eff}$ can then be approximately represented as

$$D_{\rm eff} \propto \frac{1}{(P)^{1/4}}, \tag{B5}$$

which indicates that a higher purity results in a smaller phase diffusion of the oscillator.

ORCID iDs

Yuzuru Kato https://orcid.org/0000-0001-8508-4677
Hiroya Nakao https://orcid.org/0000-0003-3394-0392

References

[1] Winfree A T 2001 *The Geometry of Biological Time* (New York: Springer)
[2] Kuramoto Y 1984 *Chemical Oscillations, Waves, and Turbulence* (Berlin: Springer)
[3] Pikovsky A, Rosenblum M and Kurths J 2001 *Synchronization: A Universal Concept in Nonlinear Sciences* (Cambridge: Cambridge University Press)
[4] Nakao H 2016 *Contemp. Phys.* **57** 188
[5] Strogatz S 1994 *Nonlinear Dynamics and Chaos* (Boulder: Westview Press)
[6] Shapiro S 1963 *Phys. Rev. Lett.* **11** 80
[7] Adler R 1946 *Proc. IRE* **34** 351
[8] Best R E 1984 *Phase-locked Loops: Theory, Design, and Applications* (New York: McGraw-Hill)
[9] Tass P A 2001 *Biol. Cybern.* **85** 343
[10] Shim S-B, Imboden M and Mohanty P 2007 *Science* **316** 95
[11] Zhang M, Wiederhecker G S, Manipatruni S, Barnard A, McEuen P and Lipson M 2012 *Phys. Rev. Lett.* **109** 233906
[12] Zhang M, Shah S, Cardenas J and Lipson M 2015 *Phys. Rev. Lett.* **115** 163902
[13] Bagheri M, Poot M, Fan L, Marquardt F and Tang H X 2013 *Phys. Rev. Lett.* **111** 213902

[14] Matheny M H, Grau M, Villanueva L G, Karabalin R B, Cross M and Roukes M L 2014 *Phys. Rev. Lett.* **112** 014101
[15] Matheny M H *et al* 2019 *Science* **363** eaav7932
[16] Colombano M *et al* 2019 *Phys. Rev. Lett.* **123** 017402
[17] Liao C-G, Chen R-X, Xie H, He M-Y and Lin X-M 2019 *Phys. Rev.* A **99** 033818
[18] Kreinberg S, Porte X, Schicke D, Lingnau B, Schneider C, Höfling S, Kanter I, Lüdge K and Reitzenstein S 2019 *Nat. Commun.* **10** 1539
[19] Singh H, Bhuktare S, Bose A, Fukushima A, Yakushiji K, Yuasa S, Kubota H and Tulapurkar A A 2019 *Phys. Rev. Appl.* **11** 054028
[20] Laskar A W, Adhikary P, Mondal S, Katiyar P, Vinjanampathy S and Ghosh S 2020 *Phys. Rev. Lett.* **125** 013601
[21] Koppenhöfer M, Bruder C and Roulet A 2020 *Phys. Rev. Res.* **2** 023026
[22] Lee T E and Sadeghpour H 2013 *Phys. Rev. Lett.* **111** 234101
[23] Walter S, Nunnenkamp A and Bruder C 2014 *Phys. Rev. Lett.* **112** 094102
[24] Kato Y, Yamamoto N and Nakao H 2019 *Phys. Rev. Res.* **1** 033012
[25] Kato Y and Nakao H 2020 *Phys. Rev.* E **101** 012210
[26] Kato Y and Nakao H 2020 arXiv:2006.00760
[27] Lörch N, Amitai E, Nunnenkamp A and Bruder C 2016 *Phys. Rev. Lett.* **117** 073601
[28] Weiss T, Walter S and Marquardt F 2017 *Phys. Rev.* A **95** 041802
[29] Sonar S, Hajdušek M, Mukherjee M, Fazio R, Vedral V, Vinjanampathy S and Kwek L-C 2018 *Phys. Rev. Lett.* **120** 163601
[30] Lee T E, Chan C-K and Wang S 2014 *Phys. Rev.* E **89** 022913
[31] Walter S, Nunnenkamp A and Bruder C 2015 *Ann. Phys., Lpz.* **527** 131
[32] Es' haqi-Sani N, Manzano G, Zambrini R and Fazio R 2020 *Phys. Rev. Res.* **2** 023101
[33] Davis-Tilley C, Teoh C K and Armour A D 2018 *New J. Phys.* **20** 113002
[34] Roulet A and Bruder C 2018 *Phys. Rev. Lett.* **121** 053601
[35] Roulet A and Bruder C 2018 *Phys. Rev. Lett.* **121** 063601
[36] Ludwig M and Marquardt F 2013 *Phys. Rev. Lett.* **111** 073603
[37] Weiss T, Kronwald A and Marquardt F 2016 *New J. Phys.* **18** 013043
[38] Amitai E, Lörch N, Nunnenkamp A, Walter S and Bruder C 2017 *Phys. Rev.* A **95** 053858
[39] Xu M, Tieri D A, Fine E, Thompson J K and Holland M J 2014 *Phys. Rev. Lett.* **113** 154101
[40] Xu M and Holland M 2015 *Phys. Rev. Lett.* **114** 103601
[41] Witthaut D, Wimberger S, Burioni R and Timme M 2017 *Nat. Commun.* **8** 14829
[42] Bastidas V, Omelchenko I, Zakharova A, Schöll E and Brandes T 2015 *Phys. Rev.* E **92** 062924
[43] Lörch N, Nigg S E, Nunnenkamp A, Tiwari R P and Bruder C 2017 *Phys. Rev. Lett.* **118** 243602
[44] Hush M R, Li W, Genway S, Lesanovsky I and Armour A D 2015 *Phys. Rev.* A **91** 061401
[45] von Neumann J 1932 *Mathematical Foundations of Quantum Mechanics* (Berlin: Springer)
[46] Nielsen M A and Chuang I L 2000 *Quantum Computation and Quantum Information* (Cambridge: Cambridge University Press)
[47] Belavkin V P 1992 *J. Multivariate Anal.* **42** 171
[48] Wiseman H M and Milburn G J 2009 *Quantum Measurement and Control* (Cambridge: Cambridge University Press)
[49] Jacobs K 2010 *New J. Phys.* **12** 043005
[50] Kato Y and Yamamoto N 2014 *New J. Phys.* **16** 023024
[51] Gu M, Parkins A and Carmichael H 2006 *Phys. Rev.* A **73** 043813
[52] Bhattacharya T, Habib S and Jacobs K 2000 *Phys. Rev. Lett.* **85** 4852
[53] Scott A and Milburn G J 2001 *Phys. Rev.* A **63** 042101
[54] Eastman J K, Szigeti S S, Hope J J and Carvalho A R 2019 *Phys. Rev.* A **99** 012111
[55] Hatridge M *et al* 2013 *Science* **339** 178
[56] Minev Z K, Mundhada S O, Shankar S, Reinhold P, Gutiérrez-Jáuregui R, Schoelkopf R J, Mirrahimi M, Carmichael H J and Devoret M H 2019 *Nature* **570** 200
[57] Hays M *et al* 2020 *Nat. Phys.* **16** 1103–7
[58] Koppenhöfer M, Bruder C and Lörch N 2018 *Phys. Rev.* A **97** 063812
[59] Chia A, Kwek L-C and Noh C 2020 *Phys. Rev.* E **102** 042213
[60] Kato Y and Nakao H Instantaneous quantum phase synchronization of two decoupled quantum limit-cycle oscillators induced by conditional photon detection (submitted) (arXiv:2009.08286)
[61] Gardiner C W 1991 *Quantum Noise* (New York: Springer)
[62] Mok W-K, Kwek L-C and Heimonen H 2020 *Phys. Rev. Res.* **2** 033422
[63] Jacobs K and Steck D A 2006 *Contemp. Phys.* **47** 279
[64] Johansson J R, Nation P D and Nori F 2012 *Comput. Phys. Commun.* **183** 1760
Johansson J R, Nation P D and Nori F 2013 *Comput. Phys. Commun.* **184** 1234
[65] Lifson S and Jackson J L 1962 *J. Chem. Phys.* **36** 2410
[66] Pikovsky A 2015 *Phys. Rev. Lett.* **115** 070602